ORIGINAL ARTICLE

Approximate decorrelation and non-isotropic smoothing of time-variable GRACE-type gravity field models

Jürgen Kusche

Abstract   We discuss a new method for approximately decorrelating and non-isotropically filtering the monthly gravity fields provided by the gravity recovery and climate experiment (GRACE) twin-satellite mission. The procedure is more efficient than conventional Gaussian-type isotropic filters in reducing stripes and spurious patterns, while retaining the signal magnitudes. One of the problems that users of GRACE level 2 monthly gravity field solutions fight is the effect of increasing noise in higher frequencies. Simply truncating the spherical harmonic solution at low degrees causes the loss of a significant portion of signal, which is not an option if one is interested in geophysical phenomena on a scale of few hundred to few thousand km. The common approach is to filter the published solutions, that is to convolve them with an isotropic kernel that allows an interpretation as smoothed averaging. The downside of this approach is an amplitude bias and the fact that it neither accounts for the variable data density that increases towards the poles where the orbits converge nor for the anisotropic error correlation structure that the solutions exhibit. Here a relatively simple regularization procedure will be outlined, which allows one to take the latter two effects into account, on the basis of published level 2 products. This leads to a series of approximate decorrelation

transformations applied to the monthly solutions, which enable a successive smoothing to reduce the noise in the higher frequencies. This smoothing effect may be used to generate solutions that behave, on average over all possible directions, very close to Gaussian-type filtered ones. The localizing and smoothing properties of our non-isotropic kernels are compared with Gaussian kernels in terms of the kernel variance and the resulting amplitude bias for a standard signal. Examples involving real GRACE level 2 fields as well as geophysical models are used to demonstrate the techniques. With the new method, we find that the characteristic striping pattern in the GRACE solutions are much more reduced than Gaussian-filtered solutions of comparable signal amplitude and root mean square.

1 Introduction

The gravity recovery and climate experiment (GRACE) mission provides measurements of the time-variable Earth gravity field (Tapley et al. 2004). Combined with simultaneous and complementary observations and model results, it enables one to quantify interactions between atmosphere, hydrosphere and geosphere. The satellite gravity observations are facilitating closure of equations expressing mass change globally and locally. On land, they provide the change in terrestrial water storage and allow in hydrography to estimate the evapo-transpiration from the terrestrial water budget (Rodell et al. 2004). At sea, they provide the change in ocean

J. Kusche
Delft Institute of Earth Observation and Space Systems (DEOS), Delft University of Technology, Kluyverweg 1, P.O. Box 5058, 2600 GB Delft, The Netherlands
e-mail: j.kusche@lr.tudelft.nl

J. Kusche (✉)
GeoForschungsZentrum Potsdam,
Department 1: Geodesy and Remote Sensing, Telegrafenberg, 14473 Potsdam, Germany
e-mail: jkusche@gfz-potsdam.de

water mass, unlike satellite radar altimetry, which cannot distinguish between steric and non-steric sea-level changes (Chambers et al. 2004).

GRACE is a twin-satellite formation, with two identical spacecraft chasing each other in similar near-polar orbits. A K-band ranging system (KBR) provides the biased intersatellite range as well as its derivatives with respect to time. In addition, both satellites are equipped with geodetic GPS receivers as well as accelerometry for removing non-gravitational forces prior to data analysis. The data reduction for GRACE is described in Flechtner (2003) and Bettadpur (2004). Unconstrained solutions are generated and published on a regular base by the Center for Space Research (CSR) at the University of Texas, GeoForschungsZentrum Potsdam (GFZ), and the Jet Propulsion Laboratory (JPL), which form the GRACE science data system (SDS).

However, due to the sensor error characteristics, the mission geometry, and possibly due to limitations in current analysis strategies and background models, these unconstrained GRACE monthly models cannot be used to their full spectral extent without modification. Being a single-orbital plane mission, the ability of GRACE to recover short-time temporal variations in gravity is limited. Schrama and Visser (2007) demonstrated the effect of background model errors on the accuracy of monthly fields based upon closed-loop simulations. In Wahr et al. (2006), error estimates were derived from non-annual variability, fitting quite well to published 'calibrated' errors. They, and many other authors, have stressed the need to smooth the GRACE models by spectral convolution with a kernel of gradually decreasing power, in order to cope with the increasing noise and artefacts ('stripes') present in the GRACE models for higher degrees. This is particularly important if geoid changes are being inverted to changes in the height of an equivalent column of water loading the Earth or the associated vertical deformation effect, because load Love numbers decrease quickly and the corresponding kernels amplify the higher degree noise even more.

Low-degree truncation is not a real solution to the problem, because one discards a larger part of the signal in this case, and it is difficult to focus on regional applications like computing basin averages. Finally, constraining or regularization of the monthly normal equations is a different option to smooth out the noise in the fields, but it is available only to those who process the actual GRACE KBR and GPS data. Regularized solutions have been provided by the GRACE SDS, mainly motivated by the fact that in September 2004 the GRACE satellites went through a 61/4 resonance orbit, thus resulting in a degraded spatial coverage around this month. Furthermore, because GRACE sci-

entific applications vary widely in their need for smoothing, one would wish to have a whole 'multiresolution' scale of smoothed versions of each individual field available. This would mean the GRACE analysis centers (ACs) would have to provide a whole set of differently constrained versions for each field to the users, which appears unlikely at the moment.

Isotropic Gaussian smoothing (i.e., degree-dependent down-weighting of the Stokes coefficients) of the GRACE monthly gravity fields had been proposed in Wahr et al. (1998), based upon methods outlined in Jekeli (1981). Swenson and Wahr (2002) refined isotropic smoothing by devising three methods where the spectral weights derive from statistical optimization principles well-known in inverse theory. The problem of the optimal degree of smoothing has also been studied e.g., by Seo and Wilson (2005), Chen et al. (2005), and these authors suggest to base the choice on a comparison with independent geophysical data in terms of the signal energy (the global root mean square (RMS)).

Fengler et al. (2006) have embedded isotropic smoothing in a formal wavelet multiresolution concept. They used a kernel with cubic-polynomial behaviour in the spectral domain for analysing GRACE models. At the same time, Schmidt et al. (2006) applied similar isotropic kernels in a direct least-squares estimate to in-situ GRACE data, circumventing the use of spherical harmonics. Han et al. (2005) devised a non-isotropic smoothing kernel whose spectral Legendre coefficients depend on both degree and order. In fact, their kernel is constructed as a Gaussian where the averaging radius varies with the harmonic order. In consequence, the Gaussian is compressed in the North-South direction as compared to the East-West direction. Finally, Swenson and Wahr (2006) designed a non-isotropic kernel in order to decorrelate the GRACE coefficients.

Smoothing the spherical harmonic solutions by convolution with a kernel that itself presents a smoothed form of the spherical Dirac kernel, may be viewed as a particular method of regularization. If one accepts this view, it is obvious that a regularization bias will be introduced: it has been noticed by several authors (e.g. Chen et al. 2005, 2006; Klees et al. 2006) that time-series of smoothed area averages of surface mass change from GRACE are being biased towards zero in amplitude (with a negligible phase shift typically if signals outside the area are removed), and some authors (Velicogna and Wahr 2006; Fenoglio-Marc et al. 2006) have tried to counteract this effect by deriving amplitude rescaling factors.

Another issue in the discussion is that if one agrees that Tikhonov-type regularization (or other constraining methods that 'improve' the original normal equations)

can be viewed under the same framework than post-analysis smoothing of the least-squares solution, one will accept that in favour of Tikhonov-type regularization, several optimality principles exist. Here, the geodetic community has extended expertise with parameter choice strategies for finding the proper degree of smoothing in a particular problem.

The approach that we pursue here is along this line: a non-isotropic two-point kernel function shall be constructed such that its application to the monthly GRACE solutions 'mimics' the Tikhonov-type regularization of the original normal equation system. To this end, a 'synthetic error covariance matrix' computed from GRACE orbits, and an a-priori signal covariance matrix will be used. As we shall see, this computation does not require particularly accurate or dense orbits or an accurate functional model of GRACE data processing. However, it does take into account the North-South correlation structure of the fields quite efficiently. The degree of smoothing itself can be modified through the weighting of the two covariances and the power-law within the signal covariance. Consequently, we call this method 'approximate decorrelation and non-isotropic smoothing'.

The paper is organized as follows: in Sect. 2, we will briefly review the conventional degree- and degree/order- dependent smoothing techniques. Then, in Sect. 3, the new method of non-isotropic smoothing by approximate decorrelation and successive regularization is introduced. This leads to two-point smoothing kernels being defined. Two performance measures that apply for isotropic and non-isotropic smoothing will be introduced in Sect. 4. Finally, on this basis, we will investigate our smoothing kernels numerically in Sect. 5. They will be applied to a set of time-variable GRACE gravity models as well as to a set of geophysical models.

2 Smoothing time-variable gravity fields: an overview

2.1 Motivation

The purpose of this section is to briefly introduce isotropic smoothing for global gravity field models, as a prerequisite for the new method to be discussed in the sequel. We will also briefly discuss degree/order-dependent, non-isotropic smoothing techniques.

Let x denote a vector containing a finite set of fully one-normalized spherical harmonic coefficients of degree l and order m, complete to degree L

$$x_{lmq} = \begin{cases} c_{lm} & \text{for } q = 1 \\ s_{lm} & q = 2 \end{cases}, \tag{1}$$

such that a finite approximation of the Earth's gravitational potential at location r, λ, θ can be written as

$$T = \frac{GM}{r} \sum_{l=0}^{L} \sum_{m=0}^{l} \sum_{q=1}^{2} \left(\frac{R}{r}\right)^l x_{lmq} \bar{Y}_{lmq} = \boldsymbol{a}^T \boldsymbol{x}, \tag{2}$$

where GM and R are the Earth's gravitational constant times mass and the reference length scale of the spherical harmonic representation, and $\bar{Y}_{lmq}(\lambda, \theta)$ are the fully normalized spherical harmonics. Let further $\hat{\boldsymbol{x}}$ be an unbiased least-squares (LS) estimate based on a month of GRACE data and referenced to a long-term mean model, and let $\hat{\boldsymbol{x}}_\gamma$ denote a smoothed version to be discussed in the following, where the numerical value of γ indicates the degree of smoothing.

Grids $z_i = z(\gamma_j, \theta_k, t)$ of geophysically relevant quantities, like monthly geoid changes or surface mass changes, collected in $\boldsymbol{z}$, are then derived by linear spectral operations $\hat{\boldsymbol{z}}_\gamma = \boldsymbol{F}\hat{\boldsymbol{x}}_\gamma$ and basin or area averages $\sigma = \sigma(t)$, e.g., of surface mass or water storage variation follow in the same way from the estimates, $\hat{\sigma}_\gamma = \boldsymbol{g}^T \hat{\boldsymbol{x}}_\gamma$. The $\boldsymbol{F}$ and $\boldsymbol{g}$ contain the spectral conversion factors or 'spherical symbols' that convert geoid change into the aforementioned quantities, as well possible spherical harmonic basin function coefficients. A discussion regarding evaluation and averaging on the ellipsoid might take place elsewhere in the literature, but is not covered here.

2.2 Degree-dependent smoothing

For degree-dependent smoothing of the gravity model, the 'filtered' spherical harmonic coefficients are simply given by

$$\hat{x}_{lmq;\gamma} = w_{l;\gamma} \hat{x}_{lmq} \tag{3}$$

or, written in matrix form ($\boldsymbol{W}_\gamma = \text{diag}(w_{l;\gamma})$),

$$\hat{\boldsymbol{x}}_\gamma = \boldsymbol{W}_\gamma \hat{\boldsymbol{x}}, \tag{4}$$

where the $w_{l;\gamma}$ are degree-dependent weighting factors, which can be given an interpretation as Legendre coefficients of an isotropic smoothing kernel

$$W_\gamma(\lambda, \theta, \lambda', \theta') = \sum_{l=0}^{\infty} \sum_{m=0}^{l} \sum_{q=1}^{2} w_{l;\gamma} \bar{Y}_{lmq}(\lambda, \theta) \bar{Y}_{lmq}(\lambda', \theta')$$

$$= \sum_{l=0}^{\infty} (2l+1) w_{l;\gamma} P_l(\cos \psi), \tag{5}$$

with $\cos \psi = \sin \theta \sin \theta' \cos(\lambda - \lambda') + \cos \theta \cos \theta'$ and P_l being unnormalized Legendre polynomials.

The smoothed gravity potential will be

$$T_\gamma(\lambda, \theta) = \int_\Omega W_\gamma(\lambda, \theta, \lambda', \theta') T(\lambda', \theta') \mathrm{d}\omega'$$

$$= \int_\Omega \delta_{W_\gamma}^{(\lambda,\theta)}(\lambda', \theta') T(\lambda', \theta') \mathrm{d}\omega' \quad (6)$$

where the integration extends over the unit sphere Ω, and

$$\delta_{W_\gamma}^{(\lambda,\theta)}(\lambda', \theta') = \int_\Omega W_\gamma(\lambda', \theta', \lambda'', \theta'') \delta^{(\lambda,\theta)}(\lambda'', \theta'') \mathrm{d}\omega''. \quad (7)$$

In Eq. (7), $\delta^{(\lambda,\theta)}$ denotes the spherical Dirac kernel located at λ, θ, and $\delta_{W_\gamma}^{(\lambda,\theta)}$ is a smoothed version of $\delta^{(\lambda,\theta)}$. The global RMS of the smoothed solution is damped by the factor

$$\alpha_{T,W_\gamma} = \frac{\hat{\boldsymbol{x}}^T \boldsymbol{W}_\gamma^T \boldsymbol{W}_\gamma \hat{\boldsymbol{x}}}{\hat{\boldsymbol{x}}^T \hat{\boldsymbol{x}}}, \quad (8)$$

which is the Rayleigh quotient of $\boldsymbol{W}_\gamma^T \boldsymbol{W}_\gamma$ in the direction of the field.

We will now relate our concept to the multiresolution scheme of Fengler et al. (2006). For the moment, we will assume that γ represents a regularization parameter controlling the 'width' of the kernel, with $T_\gamma \to T$ for $\gamma \to 0$. This is obviously the case for the kernel variance discussed in Sect. 4.1. Let $\gamma = \gamma(j)$ be associated with some integer scale parameter $j \subset \mathbb{N}_0$, such that $\gamma \to 0$ for $j \to \infty$, and let all $w_{l;\gamma} \geq 0$. Then $w_{l;\gamma}$ as a function of degree l and scale index j is called the generator of a 'scaling function' if

$$w_{0;\gamma} = 1 \quad (9)$$

$$\lim_{j \to \infty} w_{l;\gamma} = 1 \quad (10)$$

$$0 \leq w_{l;\gamma} \leq w_{l;\gamma'} \quad \text{for } j \leq j'. \quad (11)$$

The first condition (Eq. 9) says that the kernel should be globally normalized, which is useful because only then it retains the global average of a smoothed function. One the other hand, this should not remain unchallenged, because in many applications it is rather a regional average that we are interested in. We postpone the discussion of this issue to Sect. 4.2. The second condition (Eq. 10) requires the kernel to approach the spherical Dirac kernel in the limit $\gamma \to 0$, which is equivalent to T_γ approaching T. The third condition (Eq. 11) helps in establishing a hierarchy of smoothing kernels.

In the infinite-dimensional case, the $\gamma(j)$-smoothed functions $T_{\gamma(j)}$, if assumed as belonging to the space $L_2(\Omega)$ of square-integrable functions originally, constitute a hierarchy of nested function spaces $V_0 \subset V_1 \subset$

$\cdots \subset L_2(\Omega)$ with $L_2(\Omega)$ being the closure of the unification of all individual spaces V_J. This is a multiresolution scheme (cf. Freeden et al. 1998), and it is a useful property, because we can decompose every square-integrable function on the sphere then uniquely into a sum of an initial smoothed version and some 'incrementally smoothed' versions. The mentioned scaling function will be explicitly given by Eq. (5), with $\gamma = \gamma(j)$.

In the finite-dimensional case considered here, the third condition (Eq. 11) simply comes down to

$$0 \leq \alpha_{T,W_\gamma} \leq \alpha_{T,W_{\gamma'}} \quad \text{for } j \leq j' \quad (12)$$

with α according to Eq. (8) for any field T. That is, the hierarchy of kernels, indicated by $\gamma(j)$, translates itself into a monotonically increasing damping of the global RMS. Concluding, we note that (a) virtually all kernels proposed for smoothing on the sphere (e.g., Jekeli 1981; Freeden et al. 1998) fulfill these conditions, and (b) they are easy to extend to non-isotropic smoothing kernels as we will see in Sect. 3.

The most common choice with the analysis of GRACE gravity fields, popularized by Wahr et al. (1998), is the Gaussian kernel. It has been discussed together with a few other kernels in Jekeli (1981). For the Gaussian,

$$W(\psi) = 2b \frac{\mathrm{e}^{-b(1-\cos\psi)}}{1 - \mathrm{e}^{-2b}}, \quad (13)$$

with

$$b = \frac{\ln(2)}{1 - \cos(\frac{r}{R})}, \quad (14)$$

where $r = R\psi$ is the 'half-width' parameter, where the kernel drops from 1.0 at $\psi = 0$ to 0.5, which is commonly used to indicate the degree of smoothing. We will keep in mind that a more general parameter γ can be related to r and therefore write $\gamma = \gamma(r)$. The spectral weights are derived from using recursion formulae

$$\begin{aligned} w_{0;\gamma(r)} &= 1 \\ w_{1;\gamma(r)} &= \left(\frac{1+\mathrm{e}^{-2b}}{1-\mathrm{e}^{-2b}} - \frac{1}{b} \right) \\ w_{l+1;\gamma(r)} &= -\frac{2l+1}{b} w_{l;\gamma(r)} + w_{l-1;\gamma(r)}. \end{aligned} \quad (15)$$

2.3 Degree- and order-dependent smoothing

If we allow the weights in the diagonal matrix $\boldsymbol{W}_\gamma$ to depend on both spherical harmonic degree and order,

$$\hat{x}_{lmq;\gamma} = w_{lmq;\gamma} \hat{x}_{lmq} \quad (16)$$

there is now a certain flexibility that has been used in the past to design filters or regularization operators that adopt to the geographical latitude and therefore to the data density of a satellite mission. When applying this to

the spherical Dirac kernel in location λ', θ', we arrive at the corresponding non-isotropic filter function centered at the same location,

$$W_\gamma^{\lambda',\theta'}(\lambda,\theta) = \sum_{l'=0}^{\infty} \sum_{m'=0}^{l} \sum_{q'=1}^{2} w_{lmq;\gamma} \bar{Y}_{lmq}(\lambda',\theta') \bar{Y}_{lmq}(\lambda,\theta)$$

(17)

which possesses, viewed as a function of λ, θ, the spherical harmonic coefficients $w_{lmq;\gamma} \bar{Y}_{lmq}(\lambda',\theta')$.

The conditions set by Eqs. (9), (10) and (11) can be adopted to this case by requiring $w_{001;\gamma} = 1$, $w_{lmq;\gamma} \to 1$ for $\gamma \to 0$, and $w_{lmq;\gamma} \leq w_{lmq;\gamma'}$ for $j \leq j'$. If the last condition (Eq. 11) is met, a j-ordered sequence of smoothing kernels will maintain the monotonically increasing damping expressed by Eq. (12).

As mentioned before, the kernel devised by Han et al. (2005) is of the type Eq. (16). They chose $w_{lmq;\gamma} = w_{l;r(m)}$, where $w_{l;r(m)}$ is according to Eq. (15) and $r(m) = \frac{r_1 - r_0}{m_1} m + r_0$ varies linearly with m starting with given r_0 to reach a maximal value r_1 at a chosen degree m_1.

By formulating an empirical model for correlations between spherical harmonic GRACE coefficients of like parity, Swenson and Wahr (2006) designed an approximate degree- and order-dependent decorrelation filter along a similar line as we propose in Sect. 3. The weight matrix $\mathbf{W}_\gamma$ is provided by their Eq. (5). This model, however, is derived from inspecting the GRACE coefficients themselves; it is not based on assumptions on the orbital geometry or any error source. Then, for smoothing the decorrelated field, the subsequent application of Gaussian filters is proposed.

3 Non-isotropic smoothing by approximate decorrelation and regularization

For the method discussed in this article, we will conceptually go back to the LS estimation of the spherical harmonic model based on data. With the normal equations matrix $\mathbf{N}$ and right-hand side vector $\mathbf{b}$, $\hat{\mathbf{x}}$ originates from

$$\hat{\mathbf{x}} = \mathbf{N}^{-1}\mathbf{b}.$$ (18)

If we knew a prior signal covariance $E\{\mathbf{x}\mathbf{x}^T\} = \mathbf{S} = \mathbf{M}^{-1}$, and if we knew the GRACE error covariance $E\{\hat{\mathbf{x}}\hat{\mathbf{x}}^T\} = \mathbf{E} = \mathbf{N}^{-1}$, we could compute

$$\hat{\mathbf{x}}_{\gamma(1)} = (\mathbf{N} + \mathbf{M})^{-1}\mathbf{b} = (\mathbf{N} + \mathbf{M})^{-1}\mathbf{N}\hat{\mathbf{x}} = \mathbf{W}\hat{\mathbf{x}},$$ (19)

which corresponds, loosely speaking, to a Bayesian estimate.

This assumes that $\mathbf{E} = \mathbf{N}^{-1}$; however because one does not know the GRACE background model (tides,

atmospheric pressure) errors very well, this is not fulfilled but one could at least use a 'calibrated' error covariance. Smoothing monthly GRACE models through the use of Eq. (19) had been proposed by Swenson and Wahr (2002) and applied by several authors. In case the signal and error covariance depend only on the spherical harmonic degree, the resulting filter equals to what is otherwise known as a 'Wiener' filter (Sasgen et al. 2006).

Additional smoothing will be achieved through downweighting the signal covariance by a factor a

$$\hat{\mathbf{x}}_{\gamma(a)} = (\mathbf{N} + a\mathbf{M})^{-1}\mathbf{b} = (\mathbf{N} + a\mathbf{M})^{-1}\mathbf{N}\hat{\mathbf{x}} = \mathbf{W}_{\gamma(a)}\hat{\mathbf{x}},$$ (20)

which comes down to regularization of the original normal equations. However, the common GRACE user does not have access to the GRACE normal equation matrix. Moreover, for designing a filtering technique that applies to the level-2 products, it will not be required to use the original normal matrix but an easy-to-compute approximation might do as well.

The same argument holds for the signal covariance matrix, whose exact evaluation will require bringing together an extended set of realistic geophysical models. Instead, one might want to use approximations $\bar{\mathbf{E}} = \bar{\mathbf{N}}^{-1}$ and $\bar{\mathbf{S}} = \bar{\mathbf{M}}^{-1}$, and replace Eqs. (19) and (20) by

$$\hat{\bar{\mathbf{x}}}_{\gamma(1)} = (\bar{\mathbf{N}} + \bar{\mathbf{M}})^{-1}\bar{\mathbf{N}}\hat{\mathbf{x}} = \bar{\mathbf{W}}\hat{\mathbf{x}}$$ (21)

and

$$\hat{\bar{\mathbf{x}}}_{\gamma(a)} = (\bar{\mathbf{N}} + a\bar{\mathbf{M}})^{-1}\bar{\mathbf{N}}\hat{\mathbf{x}} = \bar{\mathbf{W}}_{\gamma(a)}\hat{\mathbf{x}}.$$ (22)

Let $\mathbf{E} = \bar{\mathbf{E}} + \Delta\mathbf{E}$ and $\mathbf{S} = \bar{\mathbf{S}} + \Delta\mathbf{S}$, then it is not too difficult to see that

$$\bar{\mathbf{W}}_{\gamma(a)} = \mathbf{\Gamma}_{\gamma(a)}\mathbf{W}_{\gamma(a)}$$ (23)

with

$$\mathbf{\Gamma}_{\gamma(a)} = \mathbf{I} - \mathbf{W}_{\gamma(a)}\mathbf{R}^{III} + \mathbf{W}_{\gamma(a)}\mathbf{E}(\mathbf{I} - \mathbf{R}^I)(\mathbf{I} - \mathbf{R}^{II})^{-1}\mathbf{R}^{II}\mathbf{S}^{-1},$$ (24)

and we used the abbreviations $\mathbf{R}^I = \Delta\mathbf{E}\mathbf{E}$, $\mathbf{R}^{II} = \Delta\mathbf{S}\mathbf{S}$ and $\mathbf{R}^{III} = \Delta\mathbf{E}\mathbf{S}$.

From Eqs. (23) and (24), we understand that the filter matrix $\bar{\mathbf{W}}_{\gamma(a)}$ is a distorted version of the statistically optimal but damped filter matrix $\mathbf{W}_{\gamma(a)}$, and the distortion $\mathbf{\Gamma}_{\gamma(a)}$ decreases for increased smoothing (larger a). In principle, Eqs. (23) and (24) would allow estimating the effect of using approximate covariances, if one succeeds in expressing those relative errors $\mathbf{R}^I$, $\mathbf{R}^{II}$ and $\mathbf{R}^{III}$. We do not pursue this issue further due to space limitations.

Furthermore, after some manipulations of Eq. (20), it becomes clear that

$$W_{\gamma(a)} = \left(I + (a - a') W_{\gamma(a')} N^{-1} M \right)^{-1} W_{\gamma(a')}. \qquad (25)$$

Thus, for $a' \leq a$, and a', a connected to j', j, Eq. (12) holds. The consequence is that a monotonically increasing set of a-values guarantees the monotonic decrease in the solution RMS. This is a well-known result for Tikhonov-type regularization.

With a dense matrix W_γ as defined in this section, the filtering of the spherical harmonic coefficients can be written as

$$\hat{x}_{lmq;\gamma(a)} = \sum_{l'=0}^{L} \sum_{m'=0}^{l} \sum_{q'=1}^{2} w_{lmq;\gamma(a)}^{l'm'q'} \hat{x}_{l'm'q'}. \qquad (26)$$

The $w_{lmq;\gamma(a)}^{l'm'q'}$ establish a non-isotropic two-point kernel

$$W_{\gamma(a)}(\lambda', \theta', \lambda, \theta) = \sum_{l=0}^{L} \sum_{m=0}^{l} \sum_{q=1}^{2} \sum_{l'=0}^{L} \sum_{m'=0}^{l} \sum_{q'=1}^{2} w_{lmq;\gamma(a)}^{l'm'q'}$$
$$\times \bar{Y}_{l'm'q'}(\lambda', \theta') \bar{Y}_{lmq}(\lambda, \theta). \qquad (27)$$

Applied to the spherical Dirac function in location λ', θ', the filter function becomes

$$W_{\gamma(a)}^{\lambda', \theta'}(\lambda, \theta) = W_{\gamma(a)}(\lambda', \theta', \lambda, \theta)$$
$$= \int_\Omega W_{\gamma(a)}(\lambda'', \theta'', \lambda, \theta) \, \delta^{\lambda', \theta'}(\lambda'', \theta'') \mathrm{d}\omega''$$
$$= \sum_{l=0}^{L} \sum_{m=0}^{l} \sum_{q=1}^{2} w_{lmq;\gamma(a)} \bar{Y}_{lmq}(\lambda, \theta) \qquad (28)$$

with spherical harmonic coefficients $w_{lmq;\gamma(a)} = \sum \sum \sum w_{lmq;\gamma(a)}^{l'm'q'} \bar{Y}_{l'm'q'}(\lambda', \theta')$ when viewed as a function of λ, θ.

Equation (9) can be adapted to this case by requiring $w_{001;\gamma}^{l'm'q'} = \delta_0^{l'} \delta_0^{m'} \delta_1^{q'}$. Because $W_{\gamma(0)} = I$, Eq. (10), here $w_{lmq;\gamma}^{l'm'q'} \rightarrow \delta_l^{l'} \delta_m^{m'} \delta_q^{q'}$ for $\gamma \rightarrow 0$, is automatically fulfilled. It has already been explained that Eq. (12) holds.

The coefficients $w_{lmq;\gamma(a)}^{l'm'q'}$ are not necessarily symmetric in l, l', m, m' or q, q', as the matrix $W_{\gamma(a)}$, due to Eq. (20), will not be symmetric. Consequently, the number of coefficients to be stored will be of the order L^4 for maximum degree L; using a four-byte representation, one would have to allocate about 90 Mb (250 Mb by 790 Mb) for $L = 70(90$ by $120)$, which does not pose a major problem.

4 Performance measures

4.1 Definition of a smoothing radius using the kernel variance

The smoothing properties of a kernel function are related to its localization properties in space: a 'narrow' kernel smooths less than a 'broad' kernel. It will turn out very useful to describe the localization of a non-isotropic kernel by one single number, which we may identify with the parameter γ used in an abstract sense so far. In this way, we can compare isotropic and non-isotropic kernels, or non-isotropic kernels generated in a different way. However, this disqualifies conventional measures known from the theory of radially symmetric functions on the sphere like the half-width radius (where the value of the kernel drops to 50% of its maximum value), the distance of the first zero-crossing or other definitions of the correlation length, as these measures are hardly representative for a non-symmetric function.

Instead, we will turn to the square root of the variance of the normalized squared kernel, as proposed by Narcowich and Ward (1996). The variance is the second centralized moment of a probability density function (PDF) defined on the sphere. It is an integral measure of its spreading about the expectation and it can be defined independent of introducing a particular coordinate system for mapping the surface of the sphere. The variance is independent of location for isotropic kernels; but this clearly does not hold for non-isotropic kernels.

However, in order to be able to interpret a function F as a PDF, we must enforce that this function possesses unit integral over the sphere, and it must be non-negative. Both conditions are not necessarily fulfilled with our non-isotropic kernel functions. Therefore, we will define the variance of a smoothing kernel $W_\gamma = W_\gamma^{\lambda', \theta'}(\lambda, \theta)$ via $F = \tilde{W}_\gamma^2$ (see e.g. Freeden et al. 1998), where

$$\tilde{W}_\gamma(\lambda, \theta) = \frac{1}{|W_\gamma|_{L_2(\Omega)}} W_\gamma(\lambda, \theta)$$
$$= \frac{\sum_{l=0}^{\infty} \sum_{m=0}^{l} \sum_{q=1}^{2} w_{lmq;\gamma} \bar{Y}_{lmq}(\lambda, \theta)}{\left(\sum_{l=0}^{\infty} \sum_{m=0}^{l} \sum_{q=1}^{2} w_{lmq;\gamma}^2 \right)^{1/2}} \qquad (29)$$

and we have used $w_{lmq;\gamma} = \sum \sum \sum w_{lmq;\gamma}^{l'm'q'} \bar{Y}_{l'm'q'}(\lambda', \theta')$ for general non-isotropic filters, and $w_{lmq;\gamma} = w_{l;\gamma}$ for isotropic filters.

One has to keep in mind that, due to this definition, negative side-lobes of the original kernel map into positive ones, and the resulting variance will be larger that when one would consider the central lobe of a kernel alone. It is clear that the squared normalized kernel is

non-negative and

$$\int_{\Omega} \tilde{W}_\gamma^2 \mathrm{d}\omega = |\tilde{W}_\gamma|_{L_2(\Omega)}^2 = \frac{1}{|W_\gamma|_{L_2(\Omega)}^2} \int_{\Omega} W_\gamma{}^2 \mathrm{d}\omega = 1. \quad (30)$$

The variance is defined as (Narcowich and Ward 1996)

$$\sigma^2 = \int_{\Omega} (\boldsymbol{e} - \boldsymbol{\mu})^2 \tilde{W}_\gamma^2 \mathrm{d}\omega \quad (31)$$

where $\boldsymbol{e} = (\sin\theta\cos\lambda, \sin\theta\sin\lambda, \cos\theta)^T$ is an arbitrary location on the sphere, and $\boldsymbol{\mu}$ is the expectation operator pointing to the centre of probability mass of $\tilde{W}_\gamma^2$, i.e.,

$$\boldsymbol{\mu} = \int_{\Omega} \boldsymbol{e} \tilde{W}_\gamma^2 \mathrm{d}\omega. \quad (32)$$

This centre of mass is inside the sphere (see Freeden et al. 1998, Fig. 5.5.1, for a graphical representation of the situation.) As the unit vector can be represented through the unnormalized degree-one spherical harmonics $\boldsymbol{e} = (Y_{111}, Y_{112}, Y_{101})^T$, we can write the components of $\boldsymbol{\mu}$ as

$$\begin{aligned} \mu_x &= (\tilde{W}_\gamma^2)_{111} = \int_{\Omega} \tilde{W}_\gamma^2 Y_{111} \mathrm{d}\omega \\ \mu_y &= (\tilde{W}_\gamma^2)_{112} = \int_{\Omega} \tilde{W}_\gamma^2 Y_{112} \mathrm{d}\omega \\ \mu_z &= (\tilde{W}_\gamma^2)_{101} = \int_{\Omega} \tilde{W}_\gamma^2 Y_{101} \mathrm{d}\omega. \end{aligned} \quad (33)$$

Here by $(\tilde{W}_\gamma^2)_{lmq}$ we denote the unnormalized spherical harmonic coefficients of $\tilde{W}_\gamma^2$. Because of $(\boldsymbol{e} - \boldsymbol{\mu})^2 = 1 + (\boldsymbol{\mu})^2 - 2\boldsymbol{e}^T\boldsymbol{\mu}$ and $\int -2\boldsymbol{e}^T\boldsymbol{\mu}\tilde{W}^2 \mathrm{d}\omega = -2(\boldsymbol{\mu})^2$, the variance is then

$$\sigma^2 = 1 - (\boldsymbol{\mu})^2 = 1 - \sum_{m=0}^{1}\sum_{q=1}^{2} \left((\tilde{W}_\gamma^2)_{1mq}\right)^2. \quad (34)$$

The degree-one coefficients of $\tilde{W}_\gamma^2$ in Eq. (34) could be computed through a double series employing triple integrals of spherical harmonics, relating them to the coefficients of W_γ. The triple integrals may be expressed by Wigner-3j symbols (Edmonds 1974) and computed from recursion procedures (Schulten and Gordon 1976), but this is very cumbersome as the series would have to extend to the maximum spherical harmonic degree L present in W_γ.

Instead, we apply a 'pseudo-spectral' method, where $\tilde{W}_\gamma^2$ is generated on a suitable grid on the sphere pointwise from Eq. (29). A subsequent spherical harmonic analysis provides the degree-one coefficients for Eq. (34). The square root of the variance, scaled by the Earth's radius, $R\sigma = R\sqrt{\sigma^2}$ can serve as a representative smoothing 'radius' parameter. It will be identified with the single smoothing parameter γ mentioned earlier that we will use for measuring and comparing smoothness throughout this article.

Table 1 Square root of variance for the Gaussian smoothing operator, and the scaling bias for two different area cap sizes (with maximal degree $L = 70$)

r (km)	$R\sigma$ (km)	$\beta(R\psi = 1,500\,\mathrm{km})$ (%)	$\beta(R\psi = 3,000\,\mathrm{km})$(%)
400	339	85	93
650	549	74	87
900	759	63	82
1,000	841	59	80
1,500	1,248	41	69

Table 2 Square root of variance and standard bias for the non-isotropic smoothing operator, for different a, $p = 4$, and $\lambda' = 0°$, $\theta' = 90°$

a (-)	$R\sigma$ (km)	$\beta(R\psi = 1,500\,\mathrm{km})$ (%)	$\beta(R\psi = 3,000\,\mathrm{km})$ (%)
$a = 1 \times 10^{11}$	438	97	98
$a = 1 \times 10^{12}$	556	94	97
$a = 1 \times 10^{13}$	759	89	94
$a = 1 \times 10^{14}$	1,130	79	89
$a = 1 \times 10^{15}$	1,861	57	76

Table 3 Square root of variance and standard bias for the non-isotropic smoothing operator, for different latitudes θ', $a = 1 \times 10^{13}$, $p = 4$, and $\lambda' = 0°$

θ (°)	$R\sigma$ (km)	$\beta(R\psi = 1,500\,\mathrm{km})$ (%)	$\beta(R\psi = 3,000\,\mathrm{km})$ (%)
15	1,526	94	97
30	934	92	95
45	787	91	95
60	757	90	94
75	755	90	94
90	759	89	94

For the Gaussian, we have collected this information in Table 1. We can assign $\gamma = \gamma(r) = \sigma(r)$, where r is the half-width radius in Eq. (13). For the non-isotropic kernels introduced in Sect. 3, we can assign a relation $\gamma = \gamma(a) = \sigma(a)$. It is important to bear in mind that the variance of the kernel, unlike with isotropic kernels, depends on the location on the sphere. The square root of the variance is given in Tables 2 and 3 in Sect. 5.

4.2 Definition of a standard scaling bias

Smoothing the time-variable gravity signal by means of convolution with a kernel function reduces noise, but it also suppresses parts of the signal. From Eq. (8), we have already seen the overall damping of the signal RMS. In many applications of the GRACE monthly fields, one is interested in constructing a time-series of basin-wide averages for a region of interest, and extracting annual and semi-annual amplitude and phases from this (Wahr et al. 1998).

It has been noticed that the aforementioned bias due to smoothing leads to a significant amplitude reduction in these amplitude estimates in the first place, while the phase distortion is usually small if leakage signals of the surrounding regions are removed from modelling. Velicogna and Wahr (2006) rescaled their estimates for mass loss in Antarctica by a factor of 1/0.62, while Fenoglio-Marc et al. (2006) applied 1/0.56 for the annual amplitude of non-steric sea level in the Mediterranean Sea.

While it is not surprising that this effect depends on the particular signal (in- and outside the area of interest), the smoothing kernel itself, and on the shape of the basin, it is a valid question if we can characterize and compare it here as a property of the kernel for some sort of 'standard' basin and standard signal. It appears natural to define a standard area as disc-shaped with given radius, and the standard signal as being uniform across the standard area and zero outside. The scaling bias derived in this way is intended to be representative to what can be expected for a basin-wide oscillation of a near-uniform signal in reality, although it might be too optimistic for basins with a distinct non-spherical shape.

The relative scaling bias is the ratio of the smoothed signal $T_\gamma(\lambda, \theta)$ averaged for a region $O(\lambda, \theta)$, compared to the the original non-smoothed signal $T(\lambda, \theta)$ averaged for the same region. Writing this in the general case for non-isotropic smoothing gives

$$\beta_{O,W_\gamma,T} = \frac{T_{O_{W_\gamma}}}{T_O} = \frac{\int_\Omega O\,\mathrm{d}\omega \int_\Omega O_{W_\gamma} T\,\mathrm{d}\omega}{\int_\Omega OT\,\mathrm{d}\omega \int_\Omega O_{W_\gamma}\,\mathrm{d}\omega}$$
$$= \frac{\sum_{l=0}^\infty \sum_{m=0}^l \sum_{q=1}^2 \sum_{l'=0}^\infty \sum_{m'=0}^{l'} \sum_{q'=1}^2 w_{lmq;\gamma}^{l'm'q'} o_{lmq} x_{l'm'q'}}{\sum_{l=0}^\infty \sum_{m=0}^l \sum_{q=1}^2 o_{lmq} x_{lmq}} \tag{35}$$

where o_{lmq} denotes the spherical harmonic coefficients of the basin function (one inside, zero outside), and x_{lmq} are the coefficients of the original signal $T(\lambda, \theta)$.

Here we assumed that Eq. (9) holds as discussed before for the non-isotropic case in Sect. 3, i.e., $\frac{1}{o_{001}} \sum \sum \sum w_{001;\gamma}^{l'm'q'} o_{l'm'q'} = w_{001;\gamma} = 1$. An alternative way to define the scaling bias, as quantity that should be zero in the ideal case, would be

$$\beta'_{O,W_\gamma,T} = 1 - \beta_{O,W_\gamma,T}. \tag{36}$$

From Eq. (35), all three quantities [kernel shape (through $w_{lmq}^{l'm'q'}$), basin shape (through o_{lmq}) and signal (through $x_{l'm'q'}$)] contribute to the bias. Further investigations might continue with splitting the signal spectrally into inner (target) and exterior (leakage) signal, $T(\lambda, \theta) = T^O(\lambda, \theta) + T^{\Omega/O}(\lambda, \theta)$, but we do not pursue this direction here due to lack of space. For the finite-dimensional case considered here, Eq. (35) can be summarized as

$$\beta_{O,W_\gamma,T} = \frac{\boldsymbol{o}^T \boldsymbol{W}_\gamma \boldsymbol{x}}{\boldsymbol{o}^T \boldsymbol{x}}. \tag{37}$$

Now, for a disc-shaped standard basin of radius ψ and surface area $4\pi o_{001}^{(0,0)}$, located at the North pole for simplicity,

$$O_\psi^{(0,0)}(\lambda, \theta) = \sum_{l=0}^\infty \sum_{m=0}^l \sum_{q=1}^2 o_{lmq}^{(0,0)} \bar{Y}_{lmq}(\lambda, \theta) \tag{38}$$

$$o_{l01}^{(0,0)} = \frac{1}{4\pi} \int_{\theta=0}^\psi \int_{\lambda=0}^{2\pi} \bar{Y}_{l01}(\theta, \lambda) \sin\theta\,\mathrm{d}\theta\,\mathrm{d}\lambda$$
$$= \frac{1}{2(2l+1)} \left(P_{l-1}(\cos\psi) - P_{l+1}(\cos\psi) \right) \tag{39}$$
$$o_{001}^{(0,0)} = \frac{1}{2}(1 - \cos\psi)$$

with all other $o_{lmq}^{(0,0)} = 0$. Rotating the disc instead to an arbitrary position λ', θ', we arrive at

$$O_\psi^{(\lambda',\theta')}(\lambda, \theta) = \sum_{l=0}^\infty \sum_{m=0}^l \sum_{q=1}^2 o_{lmq}^{(\lambda',\theta')} \bar{Y}_{lmq}(\lambda, \theta) \tag{40}$$

$$o_{lmq}^{(\lambda',\theta')} = o_{l01}^{(0,0)} \bar{Y}_{lmq}(\lambda', \theta'). \tag{41}$$

Note that our disc signal is not normalized to a unit integral, consequently there is no additional 'disc factor' to be considered. An area-wide standard signal of unit amplitude is characterized by

$$x_{nmq} = o_{nmq}. \tag{42}$$

The 'standard scaling bias' for a disc signal centered at λ', θ', of extension ψ, will then be

$$\beta_{O_\psi^{(\lambda',\theta')},W_\gamma,O_\psi^{(\lambda',\theta')}} = \frac{\sum_{l=0}^\infty \sum_{m=0}^l \sum_{q=1}^2 \sum_{l'=0}^\infty \sum_{m'=0}^{l'} \sum_{q'=1}^2 w_{lmq;\gamma}^{l'm'q'} o_{lmq}^{(\lambda',\theta')} o_{l'm'q'}^{(\lambda',\theta')}}{\sum_{l=0}^\infty \sum_{m=0}^l \sum_{q=1}^2 (o_{lmq}^{(\lambda',\theta')})^2}$$
$$= \frac{\sum_{l=0}^\infty \sum_{m=0}^l \sum_{q=1}^2 \sum_{l'=0}^\infty \sum_{m'=0}^{l'} \sum_{q'=1}^2 w_{lmq;\gamma}^{l'm'q'} o_{l01}^{(0,0)} \bar{Y}_{lmq}(\lambda', \theta') o_{l'01}^{(0,0)} \bar{Y}_{l'm'q'}(\lambda', \theta')}{\sum_{l=0}^\infty \sum_{m=0}^l \sum_{q=1}^2 (o_{l01}^{(0,0)})^2 (\bar{Y}_{lmq}(\lambda', \theta'))^2} \tag{43}$$

or, in brief, it will equal to the Rayleigh quotient of $\boldsymbol{W}$ in the direction of $\boldsymbol{o}$

$$\beta_{O_\psi^{(\lambda',\theta')}, W_\gamma, O_\psi^{(\lambda',\theta')}} = \frac{\boldsymbol{o}^T \boldsymbol{W} \boldsymbol{o}}{\boldsymbol{o}^T \boldsymbol{o}}. \qquad (44)$$

For the Gaussian and for our non-isotropic kernels, the corresponding scaling bias values are provided in Tables 1, 2 and 3, for discs of radius 1,500 and 3,000 km located at the equator.

In fact, one might think of maximizing the Rayleigh quotient $\beta_{O,W_\gamma,O}$ (or minimizing $\beta'_{O,W_\gamma,O}$) for a given, possibly non-spherical, area O by an appropriate choice of the $w_{lmq;\gamma(a)}^{l'm'q'}$. This is equivalent to the spherical Slepian problem (for a recent account cf. Simons and Dahlen 2006 and the references therein), and it leads to a series of Eigenvalue problems that are difficult to solve for non-spherical areas.

5 Application to GRACE monthly gravity fields and to geophysical gridded fields

5.1 Data

In what follows, the method outlined in Sect. 3 will be first applied to Level-2 GRACE monthly gravity field solutions, provided by the GRACE project. To this end, we have retrieved exemplary monthly solutions, and removed a static long-term ('mean') gravity field as a background reference. This means that our residual fields have to be considered as anomalies with respect to time.

Because this study is only concerned with the smoothing techniques, we omit details regarding the reference time, handling of dealiasing products and ocean pole tides (cf. e.g. Flechtner 2003; Bettadpur 2004), which are important in the geophysical interpretation. Furthermore, using the kernel as described in Wahr et al. (1998) or Chao (2005), including the indirect potential effect by the loading of the Earth, they have been converted to a description of equivalent water column height.

For the sake of comparison with geophysical data, gridded ocean bottom pressure (OBP) fields from the consortium for estimating the circulation and climate of the ocean (ECCO) project (Stammer et al. 1999) and gridded land hydrological fields from the land dynamics (LaD) project (Milly and Shmakin 2002) have been retrieved. Both fields are referred to the mean of year 2002, the OBP product is converted point-wise to equivalent water column change employing the relation $dh = \frac{dp}{g\rho_w}$ that connects pressure anomalies dp, gravity g, seawater density ρ_w, and water column change dh, and the resulting fields are added to produce one unified representation of the mass redistribution.

Subsequently, both the GRACE field time-series and the (overlayed) geophysical field time-series are smoothed using the method described in Sect. 3, and Gaussian filtering has been applied for comparison. Note that smoothed GRACE solutions and corresponding geophysical fields for the same time frame have been compared to each other by many authors (cf. e.g. Tapley et al. 2004), and this is not the intention of the present paper. Rather, we want to see how the new method, being designed to deal with the (approximated) GRACE error structure, performs for the GRACE fields but also for the gridded geophysical products, which, compared the GRACE products, do not appear to exhibit a strong non-isotropic signal structure.

For the construction of a synthetic dense error covariance matrix for the GRACE solutions (Sect. 5.2), we investigated two exemplary pairs of orbits: (1) GRACE A and B orbits for August 2003 with 10s sampling, kindly provided by Drazen Švehla (Technical University Munich). We deliberately removed day 240, which is also missing in the GRACE gravity field solution of this month, in order to approximate reality somewhat closer. We thus retain 30 days. (2) Level-1b GRACE A and B orbits provided by the GRACE project (through the GFZ Information System and Data Center) for May 2004 with 60s sampling. Here we removed days 140 and 145–147, retaining 27 days. However, as it turned out, the constructed smoothing kernels in Sect. 5.3 are fortunately not sensitive to the specific choice of orbit regarding accuracy, sampling, the specific month, or the consideration of missing days.

5.2 Approximate error covariance and signal covariance

Throughout this study, we use

$$(\bar{\boldsymbol{E}})_{lmq}^{l'm'q'} = \left(a_1 \int_{t_0}^{t_0+\Delta t} \left(\bar{H}_{lmq}^A(t) - \bar{H}_{lmq}^B(t) \right) \right.$$

$$\left. \times \left(\bar{H}_{l'm'q'}^A(t) - \bar{H}_{l'm'q'}^B(t) \right) dt \right)^{-1} \qquad (45)$$

as an approximation for the GRACE error covariance, where

$$\bar{H}_{lmq}^X = \left(\frac{R}{r_X(t)} \right)^l \bar{Y}_{lmq}(\lambda_X, \theta_X), \qquad (46)$$

and $X \in \{\text{GRACE } A, B\}$.

Equation (45) corresponds to the inverse normal equation matrix in case one processes the GRACE KBR inter-satellite range-rate observation following the so-called energy conservation approach (see Jekeli 1999, and the references therein). It implicitly assumes that the GRACE satellite velocities are perfectly known, which is certainly not true. Whereas this somewhat hampers the interpretation of $\boldsymbol{E}$ as a measure of the real GRACE errors, for our purposes we will retain it as it is easy to compute given a representative pair of orbits (see Sect. 5.3), it takes the orbital characteristics into account, and it matches the likely GRACE error quite well as will be elaborated below. This type of matrix and its block-diagonal relatives have been used in error propagation studies. The factor a_1 absorbs the proper scaling of the KBR inter-satellite observation, as well as a possible calibration factor.

Equation (45) was created for this study starting with degree $l = 2$ complete to degree $L = 70$. We set $w_{lmq;\gamma(a)}^{l'm',q'} = \delta_{lmq}^{l'm',q'}$ for $l < 2$ and $w_{lmq;\gamma(a)}^{l'm',q'} = 0$ for $l > L$.

It is well known that Eq. (45) exhibits a block-diagonal structure when the spherical harmonic coefficients are arranged in an order-degree scheme. In our case, the maximum correlation 0.89 within an order-block was reached for order $m = 34$ (degrees 38 and 40). Across the order-blocks, the maximum correlation is much less with 0.07 for degree/order 18/15 and 61/61 (during the review phase of this paper Srinivas Bettadpur (CSR) kindly provided a full GRACE error covariance matrix to us, for which the maximum correlation within the order-blocks was found to 0.91 and across the order-blocks to 0.16).

The signal covariance matrix is modelled as diagonal, following a power law in the spherical harmonic degree,

$$(\bar{\boldsymbol{S}})_{lmq}^{l'm'q'} = \frac{l^{-p}}{a_2}\,\delta_l^{l'}\delta_m^{m'}\delta_q^{q'}, \tag{47}$$

where p is a factor that will be chosen based on geophysical models, as discussed below. We can absorb the scaling factor a_2 by defining the regularization parameter a as

$$a = \frac{a_2}{a_1}. \tag{48}$$

The degree variances follow from Eqs. (45) and (47) as

$$(\bar{\boldsymbol{E}})_l = \frac{\sum_{m=0}^l \sum_{q=1}^2 (\bar{\boldsymbol{E}})_{lmq}^{l'm'q'}}{2l+1} \tag{49}$$

$$(\bar{\boldsymbol{S}})_l = \frac{\sum_{m=0}^l \sum_{q=1}^2 (\bar{\boldsymbol{S}})_{lmq}^{l'm'q'}}{2l+1} = \frac{l^{-p}}{a_2}. \tag{50}$$
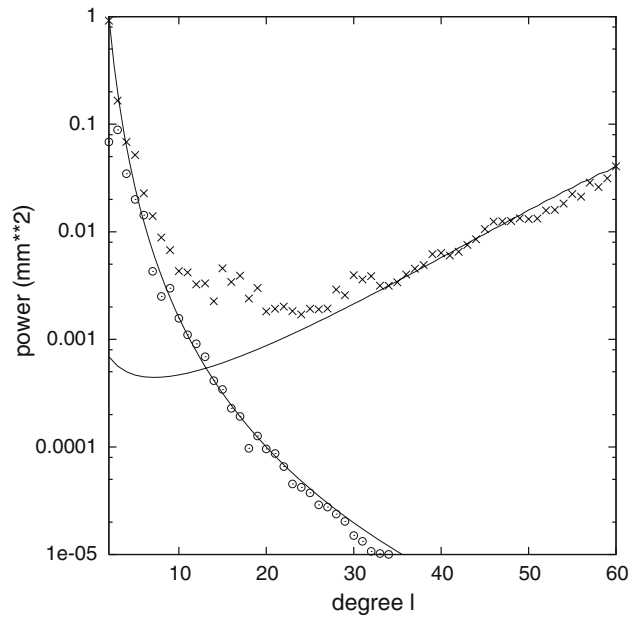
Fig. 1 Error and signal geoid power spectra (mm²): $(\bar{\boldsymbol{E}})_l$ according to Eq. (49), with $a_1 \sim 1.4 \times 10^{-15}$. $(\bar{\boldsymbol{S}})_l$ according to Eq. (50) with $p = 4$ and $a_2 = 0.0625$. Empirical signal spectrum (*circles*) according to Eq. (51) from overlay of ECCO and LaD models converted to geoid height changes. Average power (*crosses*) of monthly GRACE solution of the years 2002–2004 (the increasing branch of the spectrum may indicate the error spectrum)

Empirical signal degree variances are, correspondingly, computed from

$$c_l = \frac{\sum_{m=0}^l \sum_{q=1}^2 (x_{lmq}^{l'm'q'})^2}{2l+1}. \tag{51}$$

In Fig. 1, we show two different empirical geoid power spectra (in mm²) for the data mentioned in Sect. 5.1, as well as corresponding well-fitting models used to construct our kernels in the sequel. The circles (◦) in Fig. 1 are derived according to Eq. (51) from the overlay of the ECCO and LaD models, expanded in spherical harmonics and converted to geoid changes by applying Farrell's (1972) load Love numbers. They are used as an empirical signal spectrum here. A model $(\bar{\boldsymbol{S}})_l$ according to Eq. (50) is fitted to this spectrum, with $p = 4.0$ and $a_2 = 0.0625$. It is obvious that any $p \sim 4$ will give a good approximation. We will work with $p = 4$ for the remainder of this article.

Of course, it is questionable if the ECCO and LaD models represent the true power in the time-variable gravity field. Land hydrology and OBP are not reduced in the GRACE processing, thus these fields are expected to explain the largest part in the signal as seen by GRACE, but other contributors (e.g., post-glacial
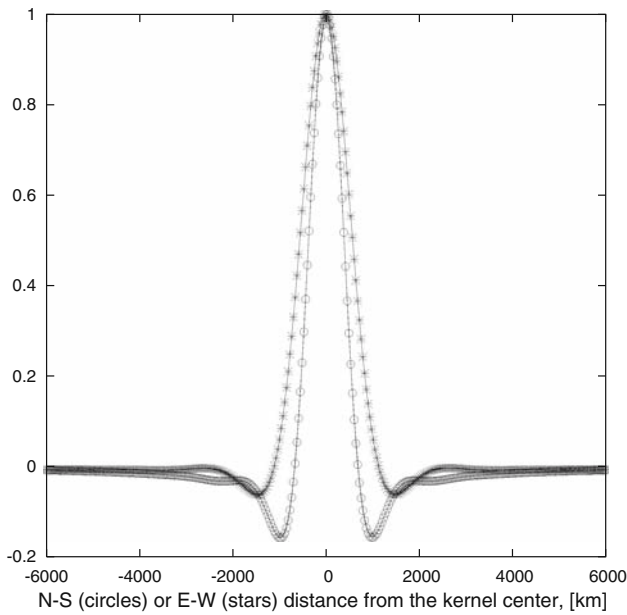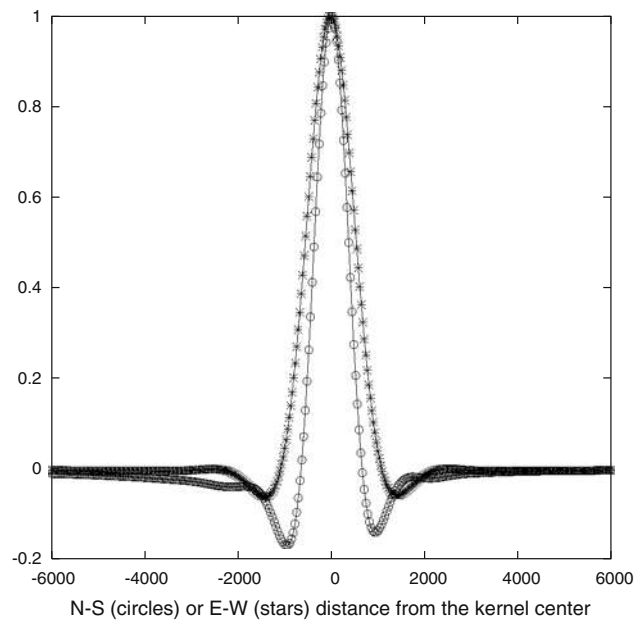
Fig. 2 Cross-section of the normalized smoothing kernel $W_{\gamma(a)}^{\lambda',\theta'}(\lambda,\theta)$, North-South (*circles*) and East-West (*asterisk*) direction; for $a = 1 \times 10^{13}$, $p = 4$, and $\lambda' = 0°$, $\theta' = 90°$. Distance (km) is measured along equator and meridian, respectively

Fig. 3 Cross-section of the normalized smoothing kernel $W_{\gamma(a)}^{\lambda',\theta'}(\lambda,\theta)$, North-South (*circles*) and East-West (*asterisk*) direction; for $a = 1 \times 10^{13}$, $p = 4$, and $\lambda' = 0°$, $\theta' = 60°$. Distance (km) is measured along equator and $\theta' = 60°$-parallel, respectively

rebound a.k.a. glacial isostatic adjustment) exist. However, we expect that our method is not overly sensitive towards misspecifications in the signal covariance.

The crosses ($\times$) in Fig. 1 are derived as the averaged power in the individual monthly GRACE solutions from analysing the years 2002–2004. It is very likely that the increasing branch of this spectrum—beyond about degree 24—is dominated by noise, as all geophysical models exhibit decreasing power for increasing harmonic degree. However, it appears very difficult to make a similar statement concerning the low-degree decreasing branch of the spectrum, as there is little validation possibility for GRACE. Assuming tacitly that the increasing branch represents the higher-degree part of the GRACE error spectrum, we can try to adjust the synthetic error covariance matrix (Eq. 45) to it by varying a_1 in a way that $(\bar{E})_l$ (Eq. 49) matches the empirical spectrum. This is the case for $a_1 \sim 1.4 \times 10^{-15}$, shown in Fig. 1.

From these fits, we may assume that an a somewhere in the order of $\sim 10^{13}$ will provide the 'optimal' non-isotropic (Swenson and Wahr 2002) kernel, which equals to the 'Wiener' filter in the terminology of Sasgen et al. (2006) for isotropic smoothing. However, several assumptions were involved in coming up with this number, as discussed before, and in our exemplary computations it will become clear that a somewhat stronger smoothing appears visually superior.

5.3 Non-isotropic smoothing kernels

Figures 2, 3, 4, 5, 6 show cross-sections of the smoothing kernels $W_{\gamma(a)}^{\lambda',\theta'}(\lambda,\theta)$ that we constructed on the sphere in the way described before, centered at location λ', θ'. For better comparison, all kernels are normalized before drawing (scaled by $1/W_{\gamma(a)}^{\lambda',\theta'}(\lambda',\theta')$). In Figs. 2, 3, 4, the kernel for fixed parameter a and p is located on different parallels along the $\lambda' = 0°$ meridian. The North-South (N-S) cross-section $W_{\gamma(a)}^{\lambda',\theta'}(\lambda',\theta)$ is drawn along this meridian, but the East-West (E-W) cross-section $W_{\gamma(a)}^{\lambda',\theta'}(\lambda,\theta')$ is constructed along the corresponding parallel for ease of interpretation. This means that a part of the difference in the cross-sections is due to the meridional convergence.

However, from Fig. 2, showing the kernel located at the equator, a few general properties of our kernels become quite obvious: The kernel is 'tighter' in the N-S direction than in E-W direction, which is clearly due to the GRACE error structure modelled in the covariance matrix. It possesses negative sidelobes, which are much more pronounced for the N-S direction than for the E-W direction. Negative sidelobes mean that the estimated, unregularized gravity field for these regions gets a negative weight in the convolution procedure: the field which is correlated in N-S direction due to track direction is decorrelated. One can understand this in the following
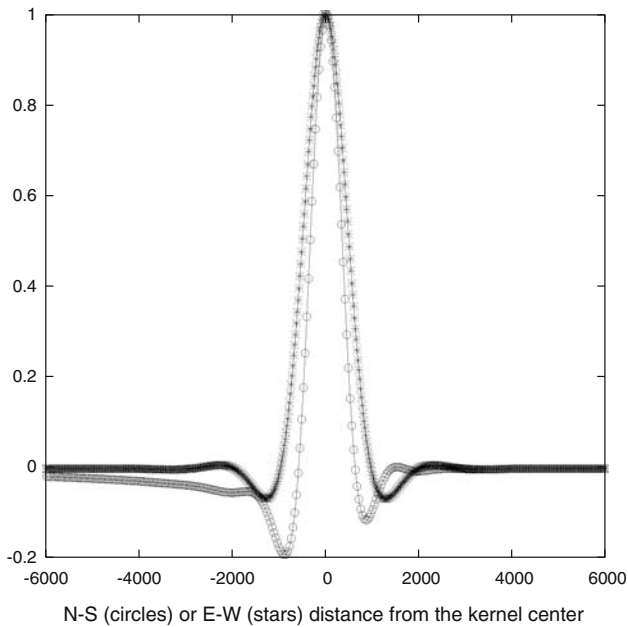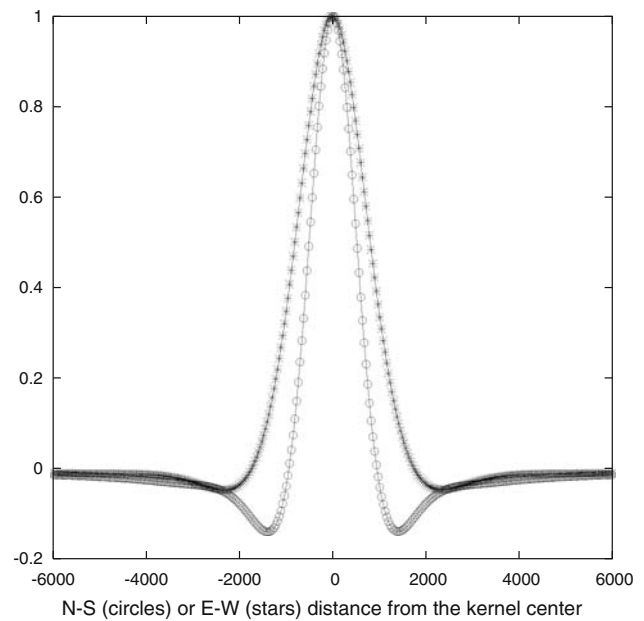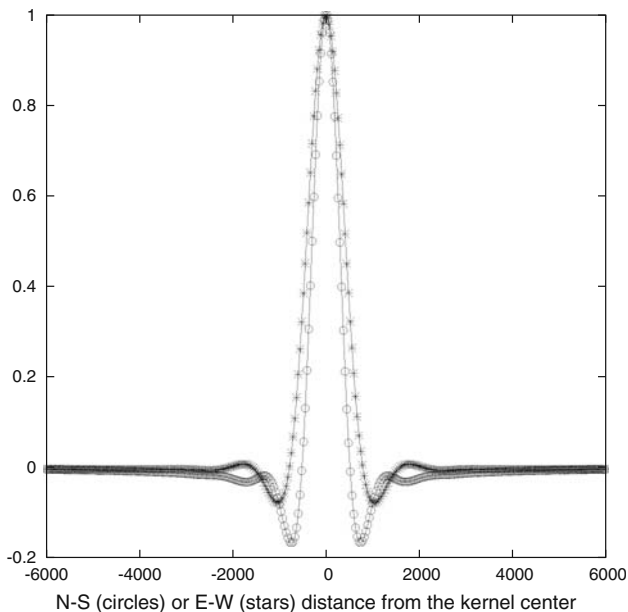
Fig. 4 Cross-section of the normalized smoothing kernel $W_{\gamma(a)}^{\lambda',\theta'}(\lambda,\theta)$, North-South (*circles*) and East-West (*asterisk*) direction; for $a = 1 \times 10^{13}$, $p = 4$, and $\lambda' = 0°$, $\theta' = 30°$. Distance (km) is measured along equator and $\theta' = 30°$-parallel, respectively

Fig. 6 Cross-section of the normalized smoothing kernel $W_{\gamma(a)}^{\lambda',\theta'}(\lambda,\theta)$, North-South (*circles*) and East-West (*asterisk*) direction; for $a = 1 \times 10^{14}$, $p = 4$, and $\lambda' = 0°$, $\theta' = 90°$. Distance (km) is measured along equator and meridian, respectively

Fig. 5 Cross-section of the normalized smoothing kernel $W_{\gamma(a)}^{\lambda',\theta'}(\lambda,\theta)$, North-South (*circles*) and East-West (*asterisk*) direction; for $a = 1 \times 10^{12}$, $p = 4$, and $\lambda' = 0°$, $\theta' = 90°$. Distance (km) is measured along equator and meridian, respectively

way: a positive correlation may be seen as a bias, and convolution with a kernel possessing negative sidelobes is equivalent to applying a differentiation filter, which removes the bias.

Negative sidelobes also exist for the kernel designed by Swenson and Wahr (2006, cf. Fig. 4). This is a clear difference to the non-isotropic Gaussian proposed by Han et al. (2005), which will always result in positive weights in all directions. One may further compare with the isotropic kernels shown in Schmidt et al. (2006, Figs. 2, 3, 4, 5), or Fengler et al. (2006, Fig. 2), which possess similar negative sidelobes but are, in contrast to our kernels, isotropic and generated from a function that analytically prescribes their Legendre coefficients.

When moving towards higher latitudes (Figs. 3 and 4), the E-W cross-section changes little—apart from the mentioned meridional convergence effect in our projection—but the N-S profile gets asymmetric in that the negative sidelobe facing the pole decreases and the one facing the equator increases in magnitude. Again, we can ascribe this to the error structure modelled in Eq. (45).

In Figs. 5 and 6, the kernel is again located at the equator but the parameter *a* is decreased and increased by one order of magnitude. Compared with Fig. 2, it becomes clear that this parameter controls the overall smoothing effect and can be used much in the same way as the half-width radius for the Gaussian kernel, thus adapting the smoothing to the desired application. We will quantify this effect in Sect. 5.4 using the variance of the non-isotropic kernel as a measure for smoothness.
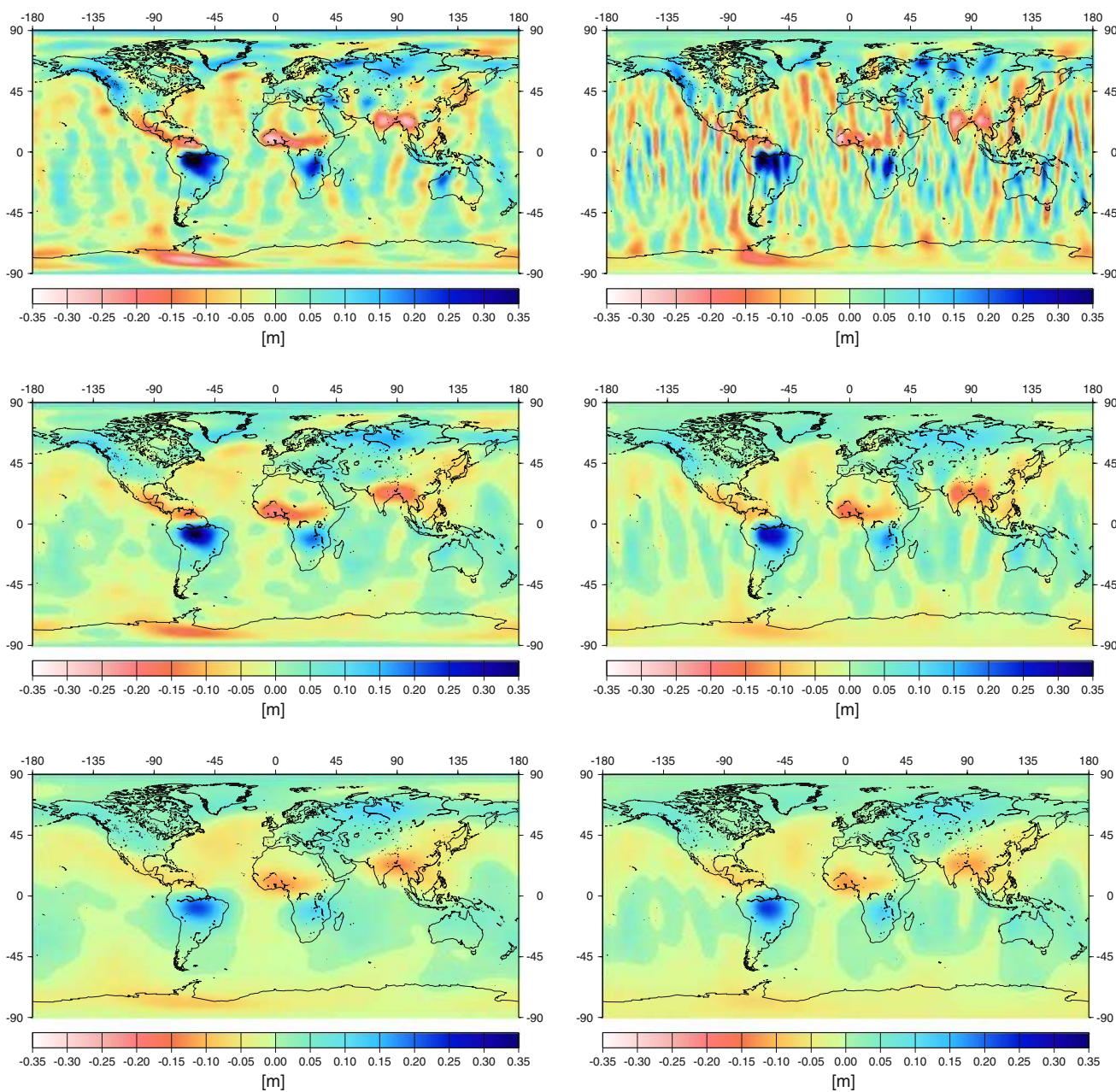
Fig. 7 Non-isotropically (*left*) and Gaussian (*right*) smoothed GRACE field, converted to equivalent water height, May 2003. From *top* to *bottom*, *left column*: $a = 10^{13}$ (max $= 0.52$ m, RMS $= 0.07$ m), $a = 10^{14}$ (max $= 0.38$ m, RMS $= 0.05$ m), $a = 10^{15}$ (max $= 0.23$ m, RMS $= 0.04$ m). From *top* to *bottom*, *right column*: half-width radius 400 km (max $= 0.45$ m, RMS $= 0.07$), 650 km (max $= 0.30$, RMS $= 0.05$), 900 km (max $= 0.23$ m, RMS $= 0.04$ m)

Finally, we have compared the kernel shown in Fig. 1 when computed using the two sets of GRACE orbits as mentioned in Sect. 5.1. The parameter a had to be scaled by a factor of $\frac{30}{27} \times 6$ to account for the different number of epochs (30 days at 10 s sampling versus 27 days at 60 s sampling) used in the evaluation of Eq. (45), but then the two corresponding kernels match each other with less than 2% difference overall. Thus, we decide that it makes no significant difference what orbit is used, even if these orbits belong to different months. This is not

surprising as the actual track structure, which does become visible in geoid error plots from Eq. (45), maps itself in the very high degrees that are efficiently damped by our kernels.

5.4 Smoothing radius and scaling bias

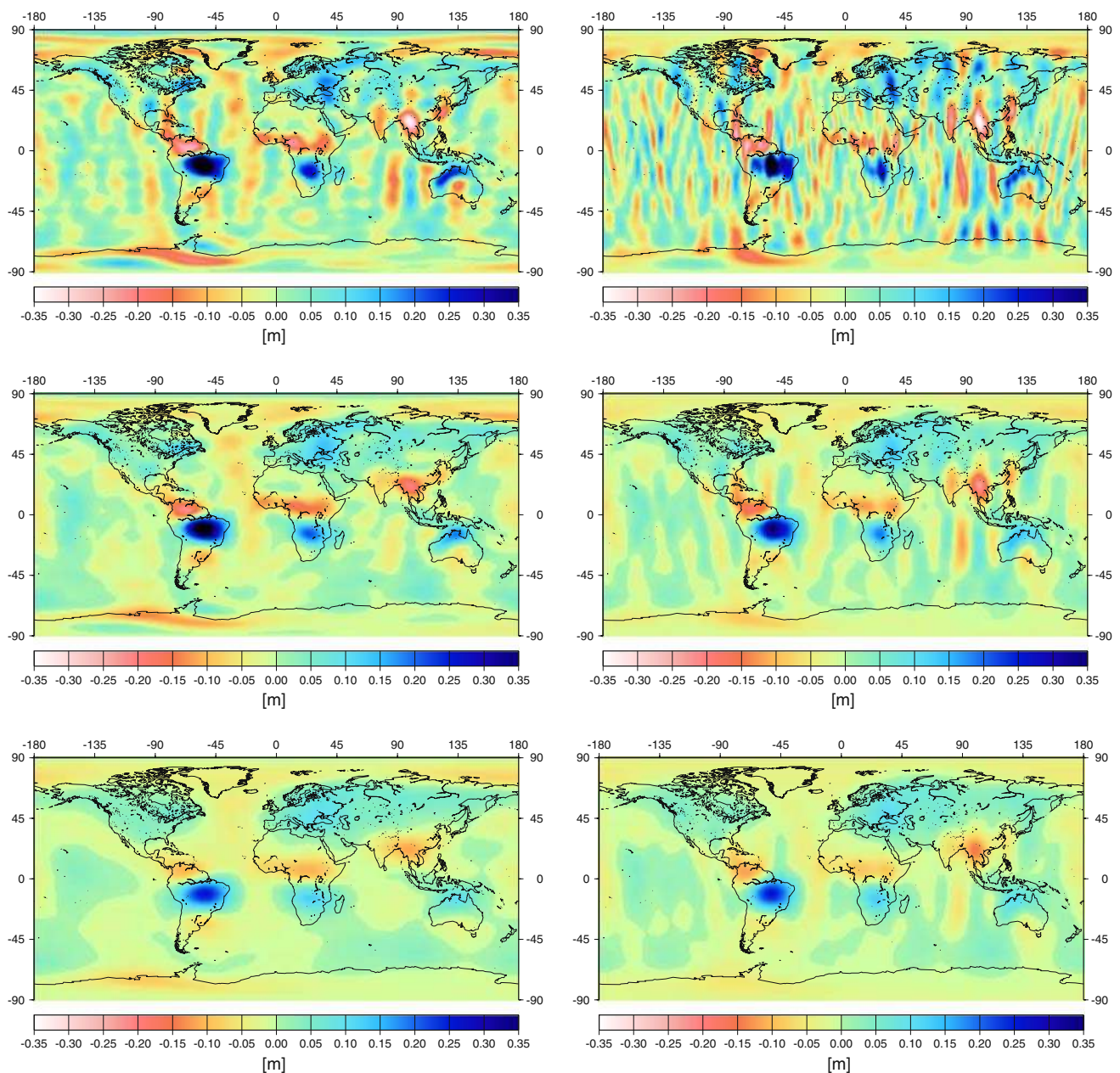Tables 2 and 3 summarize the computation of the square root of the kernel variance and the standard scaling

Fig. 8 Non-isotropically (*left*) and Gaussian (*right*) smoothed GRACE field, converted to equivalent water height, March 2004. From *top* to *bottom*, *left column*: $a = 10^{13}$ (max = 0.52 m, RMS = 0.07 m), $a = 10^{14}$ (max = 0.44 m, RMS = 0.05 m), $a = 10^{15}$ (max = 0.26 m, RMS = 0.04 m). From *top* to *bottom*, *right column*: half-width radius 400 km (max = 0.56 m, RMS = 0.08), 650 km (max = 0.36, RMS = 0.05), 900 km (max = 0.26 m, RMS = 0.04 m)

bias for several versions of our non-isotropic smoothing kernel. We have varied the smoothing parameter a, the latitude of the kernel location, and the radius of the standard basin. A radius of 1,500 km corresponds roughly to a basin the size of the Mediterranean Sea (Fenoglio-Marc et al. 2006). The variance follows from Eq. (34) and the standard bias from Eq. (43).

A comparison with Table 1 is instructive, as it reveals in how far a non-isotropic kernel corresponds to a Gaussian either of equal variance or of equal standard bias, and for which latitude. For example, at the equator, the non-isotropic kernel for $a = 10^{13}$ corresponds to a Gaussian of half-width 900 km in terms of variance but it exhibits a smaller bias as β is closer to one. Generally the
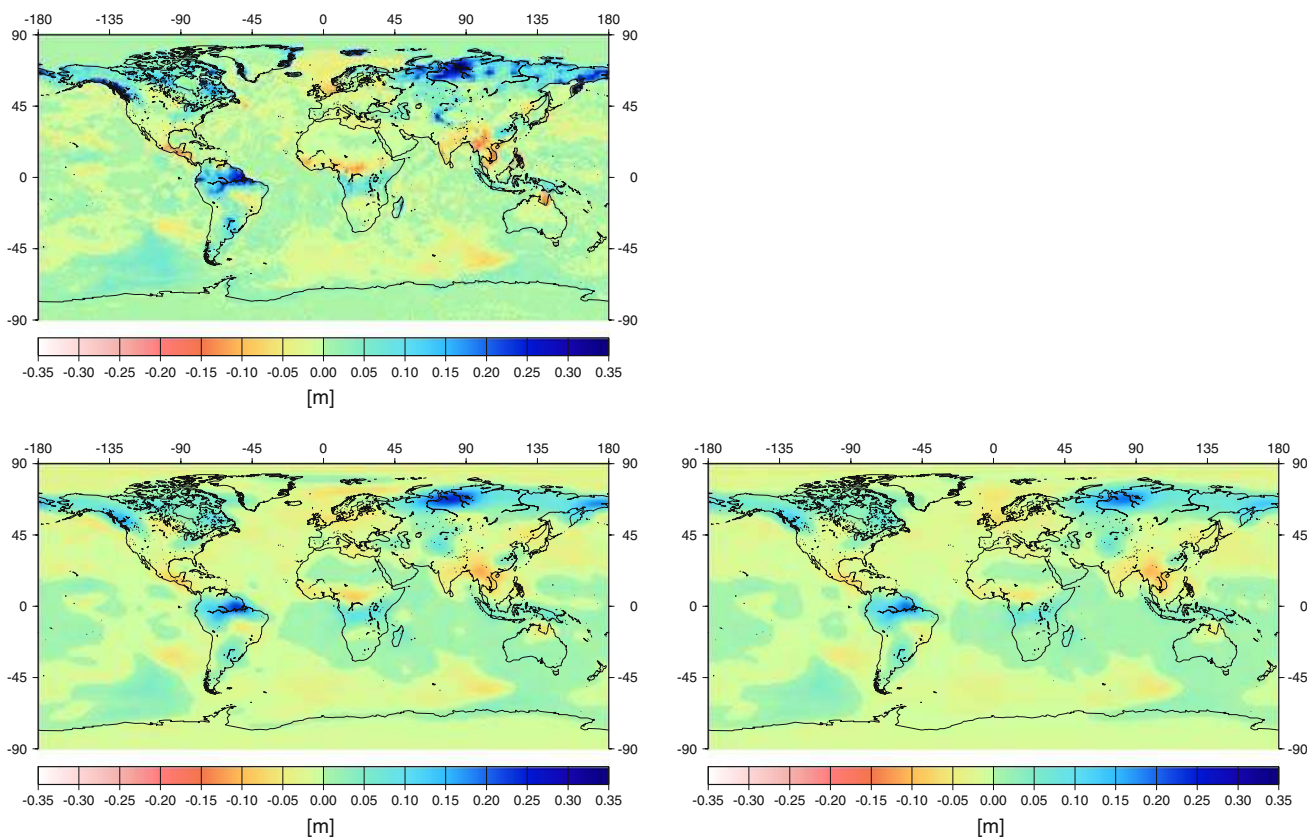
Fig. 9 Original (*top*), non-isotropically (*bottom left*) and Gaussian (*bottom right*) smoothed geophysical surface mass field, March 2002. *Top*: (max = 0.55 m, RMS = 0.04), *bottom left*: $a = 10^{14}$ (max = 0.20 m, RMS = 0.027 m), *bottom right*: 650 km (max = 0.20, RMS = 0.027)

standard bias for the non-isotropic kernels considered here is smaller than for the Gaussian.

5.5 Non-isotropically smoothed GRACE monthly models

In this section, we have applied both the new non-isotropic technique (Sects. 3 and 5.2) and the Gaussian smoothing to exemplary GRACE solutions (May 2003 and March 2004) of the first release provided by the GRACE project. These solutions suffered from large oscillations in the degree-2 coefficients so we have removed these from the plot. Consequently, all plots in Fig. 7 (8) show the same May 2003 (March 2004) GRACE gravity solution, referred to a mean field, for degrees $l = 3, \ldots, 70$ and converted to equivalent water height changes in metres. In the left column of Figs. 7 and 8, smoothing using the non-isotropic method with $a = 10^{13}$, $a = 10^{14}$ and $a = 10^{15}$ was applied; in the right column, the smoothed results for Gaussian kernels with 400, 650 and 900 km half-width are provided.

It is difficult to compare these plots visually in a comprehensive way. It has to be mentioned that the left–right correspondence of plots in Figs. 7 and 8 is chosen somewhat arbitrary based on the global RMS of the signal, as we cannot uniquely assign a certain Gaussian filter to a non-isotropic one. This is, $\alpha_{T,W_{\gamma(a)}}$ for the left columns equals approximately to $\alpha_{T,W_{\gamma(r)}}$ in the right column.

What can be said without doubt is that for the non-isotropically filtered fields, the signal magnitude (maximum and RMS values as given in the captions of Figs. 7 and 8) appears stronger than for the corresponding Gaussian-filtered field, whereas the background North-South stripings are damped much more. This is the main result of this paper. However, it is also obvious that the equatorial kernel variance, being much the same for the top left and bottom right plot of Figs. 7 and 8, fails to indicate which Gaussian and non-isotropic filter correspond to each other visually, or in terms of reduced global RMS.

5.6 Non-isotropically smoothed geophysical gridded fields

For a comparison, we have also smoothed a geophysical gridded field from ECCO/LaD (March 2002) in the

same way. These products are not 'error-free', but they are not supposed to exhibit a similar directional error structure (stripes) like the GRACE products. Moreover, the geophysical products are not excessive in amplitude as the non-smoothed GRACE fields are when converted in surface mass.

Figure 9 illustrates the original field, which was then expanded in spherical harmonics and subsequently filtered. Again, the chosen parameter *a* and the Gaussian radius *r* were matched to produce results of comparable signal RMS, although the correspondence is now different from the previous GRACE example. The results are very close, and it does not appear that true longitudinal structures (if any) are oversmoothed by the non-isotropic method.

6 Concluding remarks

We have described a new method for the approximate decorrelation and non-isotropic smoothing of GRACE monthly solutions. Smoothing is necessary due to the error structure in these gravity fields.

Our method differs from previous proposals in that it uses an approximate, fully populated, but easily computable error covariance matrix and that it employs a set of regularizations of the spherical harmonic coefficients. The smoothing kernels that follow from this setting are non-isotropic, tighter in N-S direction compared to E-W direction, and they possess negative sidelobes that depend in amplitude on the geographical latitude. The kernels are generally position-dependent. As a result, the predominant North-South error structure in the GRACE fields is approximately decorrelated. We find that the striping patterns are much more reduced than in Gaussian filtered solutions of comparable signal amplitude and RMS. This is the main result of this paper. For two exemplary monthly fields, this is clearly demonstrated here.

In contrast, for a gridded geophysical field assumed as error-free, the non-isotropic smoothing and the Gaussian smoothing lead to visually very similar results. There is however no unique one-to-one correspondence between the smoothed fields resulting from the two techniques; this makes direct comparisons difficult. Also, the proposed smoothing kernels depend on a tuning parameter that is less straightforward to interpret compared to, e.g., a Gaussian smoothing radius.

References

Bettadpur S (2004) UTCSR level-2 processing standards document for product release 01, GRACE Proj. Doc. JPL 327-742, rev. 1.1, Jet Propulsion Labaratory, Pasadena

Chambers DP, Wahr J, Nerem RS (2004) Preliminary observations of global ocean mass variation with GRACE. Geophys Res Lett 31:L13310. doi:10.1029/2004GL020461

Chao BF (2005) On inversion for mass distribution from global (time-variable) gravity field. Geophys J Int 39:223–230

Chen JL, Wilson CR, Famiglietti JS, Rodell M (2005) Spatial sensitivity of the gravity recovery and climate experiment (GRACE) time-variable gravity observations. J Geophys Res. doi:10.1029/2004JB003536

Chen JL, Wilson CR, Famiglietti JS, Rodell M (2006) Attenuation effect on seasonal basin-scale water storage changes from GRACE time-variable gravity. J Geod. doi:10.1007/s00190-006-0104-2

Edmonds AR (1974) Angular momentum in quantum mechanics. Princeton University Press, Princeton

Farrell WE (1972) Deformation of the Earth by surface loads. Rev Geophys Space Phys 10(3):761–797

Fengler MJ, Freeden W, Kohlhaas A, Michel V, Peters T (2006) Wavelet modelling of regional and temporal variations of the Earth's gravitational potential observed by GRACE. J Geod. doi:10.1007/s00190-006-0040-1

Flechtner F (2003) GFZ level-2 processing standards document for product release 01, GRACE Proj. Doc. JPL 327-743, rev. 1.0, Jet Propulsion Labaratory, Pasadena

Freeden W, Gervens T, Schreiner M (1998) Constructive approximation on the sphere. Clarendon Press, Oxford

Fenoglio-Marc L, Kusche J, Becker M (2006) Mass variation in the Mediterranean Sea from GRACE and its validation by altimetry, steric and hydrology fields. Geophys Res Lett 33:L19606. doi:10.1029/2006GL026851

Han S-C, Shum CK, Jekeli C, Kuo C-Y, Wilson CR, Seo K-W (2005) Non-isotropic filtering of GRACE temporal gravity for geophysical signal enhancement. Geophys J Int 163:18–25. doi:10.1111/j.1365-246X.2005.02756.x

Jekeli C (1981) Alternative methods to smooth the Earth's gravity field. Report No. 327, Department of Geodetic Science, Ohio State University, Ohio

Jekeli C (1999) The determination of gravitational potential differences from satellite-to-satellite tracking. Cel Mech Dyn Astr 75:85–100

Klees R, Zapreeva EA, Winsemius HC, Savenije HHG (2006) The bias in GRACE estimates of continental water storage variations. Hydrol Earth System Sci Discussions 3: 3557–3594

Narcowich FJ, Ward JD (1996) Nonstationary wavelets on the m-sphere for scattered data. Appl Comp Harm Anal 3: 324–336

Milly PCD, Shmakin AB (2002) Global modeling of land water and energy balances, Part I: The land dynamics (LaD) model. J Hydrometerol 3:283–299

Rodell M, Famiglietti JS, Chen J, Seneviratne SI, Viterbo P, Holl S, Wilson CR (2004) Basin scale estimates of evapotranspiration using GRACE and other observations. Geophys Res Lett 31:L20504. doi:10.1029/ 2004GL020873

Sasgen I, Martinec Z, Fleming K (2006) Wiener optimal filtering of GRACE data. Stud Geophys Geod 50(4):499–508. doi:10.1007/s11200-006-0031-y

Schmidt M, Fengler M, Mayer-Gürr T, Eicker A, Kusche J, Sánchez L, Han S-C (2006) Regional gravity modelling in terms of spherical base functions. J Geod 81:17–38. doi:10.1007/s00190-006-0101-5

Schrama EJO, Visser P (2007) Accuracy assessment of the monthly GRACE geoids based upon a simulation. J Geod 81(1):67–80. doi:10.1007/s00190-006-0085-1

Schulten K, Gordon RG (1976) Recursive evaluation of 3*j* and 6*j* coefficients. Comp Phys Comm 11:269–278

Seo K-W, Wilson CR (2005) Simulated estimation of hydrological loads from GRACE. J Geod. doi:10.1007/s00190-004-0410-5

Simons FJ, Dahlen FA (2006) Spherical Slepian functions and the polar gap in geodesy. Geophys. J Int 166(3):1039–1061, doi:10.1111/j.1365-245X.2006.03065.x

Stammer D, Davis R, Fu L-L, Fukomori I, Giering R, Lee T, Marotzke J, Marshall J, Menemnlis D, Niiler P, Wunsch C, Zlotnicky V (1999) The consortium for estimating the circulation and climate of the ocean (ECCO)— science goals and task plan. ECCO Report No. 1, 1999, The ECCO Consortium, La Jolla

Swenson S, Wahr J (2002) Methods for inferring regional surface-mass anomalies from gravity recovery and climate experiment (GRACE) measurements of time-variable gravity. J Geophys Res. doi:10.1029/2001JB000576

Swenson S, Wahr J (2006) Post-processing removal of correlated errors in GRACE data. Geophys Res Lett 33:L08402. doi:10.1029/2005GL025285

Tapley B, Bettadpur S, Watkins M, Reigber C (2004) The gravity recovery and climate experiment: mission overview and early results. Geophys Res Lett 31:L09607. doi:10.1029/2004GL019920

Velicogna I, Wahr J (2006) Measurements of time-variable gravity show mass loss in Antarctica. Scienceexpress, published online 2 March 2006. doi:10.1126/science.1123785

Wahr J, Molenaar M, Bryan F (1998) Time variability of the Earth's gravity field: hydrological and oceanic effects and their possible detection using GRACE. J Geophys Res 103(B12):30205–30230

Wahr J, Swenson S, Velicogna I (2006) Accuracy of GRACE mass estimates. Geophys Res Lett 33:L06401. doi:10.1029/2005GL025305